

Contents lists available at ScienceDirect

Scripta Materialia

journal homepage: www.elsevier.com/locate/scriptamat

Regular Article

Thermal expansion of Ti-Al-N and Cr-Al-N coatings

M. Bartosik^{a,b,*}, D. Holec^{b,c}, D. Apel^d, M. Klaus^d, C. Genzel^d, J. Keckes^e, M. Arndt^f, P. Polcik^g, C.M. Koller^{a,b}, P.H. Mayrhofer^{a,b}^a Institute of Materials Science and Technology, TU Wien, A-1060 Vienna, Austria^b Christian Doppler Laboratory for Application Oriented Coating Development, TU Wien, A-1060 Vienna, Austria^c Department of Physical Metallurgy and Materials Testing, Montanuniversität Leoben, A-8700 Leoben, Austria^d Helmholtz-Zentrum Berlin für Materialien und Energien, 12489 Berlin, Germany^e Department of Materials Physics, Montanuniversität Leoben, A-8700 Leoben, Austria^f Oerlikon Balzers, Oerlikon Surface Solutions AG, LI-9496 Balzers, Liechtenstein^g Plansee Composite Materials GmbH, D-86983 Lechbruck am See, Germany

ARTICLE INFO

Article history:

Received 11 August 2016

Received in revised form 14 September 2016

Accepted 15 September 2016

Available online 25 September 2016

Keywords:

Thermal expansion

TiN

CrN

Ti-Al-N

Cr-Al-N

AlN

Ab initio

ABSTRACT

The thermal expansion coefficients (TECs) of B1 structured $Ti_{1-x}Al_xN$ and $Cr_{1-x}Al_xN$ thin films – investigated by synchrotron X-ray diffraction from room temperature to 600 °C – excellently agree with *ab initio* obtained temperature dependent calculations only if they were annealed at 600 °C. As-deposited thin films, with their built-in structural defects show a lower temperature dependence of their TECs and higher values. Furthermore, our data clearly show that the TECs of cubic $Ti_{1-x}Al_xN$ and $Cr_{1-x}Al_xN$ increase with increasing Al content, and that the TEC of wurtzite type B4 structured AlN is only about half of that of B1 AlN.

© 2016 Acta Materialia Inc. Published by Elsevier Ltd. This is an open access article under the CC BY license (<http://creativecommons.org/licenses/by/4.0/>).

$Ti_{1-x}Al_xN$ and $Cr_{1-x}Al_xN$ alloys are among the most widely used physical and chemical vapor deposited hard coating materials due to their outstanding functional properties. Within these supersaturated pseudo-binary alloys, Al randomly substitutes for Ti or Cr on the metal sublattice of face-centered cubic (B1) TiN or CrN lattices leading to superior mechanical properties (e.g., by solid solution hardening), oxidation resistance, and thermal stability as compared with their binary counterparts [1,2]. Typically, the performance directly increases with increasing Al content up to a critical value of $x \sim 0.7$, where the films no longer crystallize in the desired metastable B1 structure. The crystallization of the hexagonal wurtzite type (B4) structure – for higher Al contents – generally leads to reduced mechanical properties. The self-hardening effect of B1 $Ti_{1-x}Al_xN$ by spinodal decomposition above ~ 800 °C [3] is a major basis of its extraordinary performance, and hence part of its commercial success. Annealing to higher temperatures leads to the phase transformation of the spinodally-formed AlN-rich cubic domains to their thermodynamically stable wurtzite B4 AlN structure [3]. This decomposition process – but also other important coating behaviours like crack formation and film delamination [4] – are massively

influenced by stresses present. Here, the thermal expansion coefficient (TEC) of the coating and phases present plays a crucial role.

The thermal expansion coefficient mismatch, ΔTEC , between individual phases, coating and substrate, leads to differential thermal contraction and expansion stresses upon cooling and heating, respectively. Such temperature cycles occur, e.g., during cooling down from the deposition temperature or due to friction between coated tool and workpiece [5,6]. Especially within multilayer films, the ΔTEC s of layer materials and substrate can lead to periodic residual stress fields along the film thickness. Consequently, the detailed description of the stresses present, for example by finite element methods, is also in need of detailed TECs of individual phases. Therefore, we study in detail the temperature dependent thermal expansion coefficient of $Ti_{1-x}Al_xN$ and $Cr_{1-x}Al_xN$ alloys by high-temperature X-ray diffraction and Density Functional Theory.

Various $Ti_{1-x}Al_xN$ and $Cr_{1-x}Al_xN$ coatings were prepared using a batch-type Oerlikon Balzers Innova deposition system equipped with 6 in. Ti , $Ti_{0.50}Al_{0.50}$, Cr , $Al_{0.50}Cr_{0.50}$, $Al_{0.60}Cr_{0.40}$, and $Al_{0.70}Cr_{0.30}$ targets (prepared by powder-metallurgy, Plansee Composite Materials GmbH), respectively. The substrates (low alloyed steel foil) were positioned parallel to the cathode surface at a distance of ~ 25 cm (no substrate rotation), heated to ~ 300 °C, and biased with -80 V DC during the 60 min deposition time. The $Cr_{1-x}Al_xN$ coatings were sputter

* Corresponding author at: Institute of Materials Science and Technology, TU Wien, A-1060 Vienna, Austria.

E-mail address: matthias.bartosik@tuwien.ac.at (M. Bartosik).

deposited by powering the $\text{Cr}_{1-x}\text{Al}_x$ cathodes with 5 kW DC within an Ar/N_2 gas mixture (Ar flow rate of 238 sccm and regulating the nitrogen pressure to have a total deposition pressure of ~ 1.1 Pa). The $\text{Ti}_{1-x}\text{Al}_x\text{N}$ coatings were sputter deposited by powering the $\text{Ti}_{1-x}\text{Al}_x$ cathodes with 4 kW DC within an Ar/N_2 gas mixture (Ar flow rate of 238 sccm and regulating the nitrogen pressure to have a total deposition pressure of ~ 1.4 Pa). After the deposition, the low-alloyed steel foils were chemically dissolved in diluted nitric acid to obtain free-standing as-deposited coating materials, which were carefully ground to powders. The chemical compositions of the films were determined by a Philips XL-30 scanning electron microscope equipped with an EDAX Sapphire Energy Dispersive X-ray detector. The EDX measurements were calibrated with thin film standards characterized by elastic recoil detection analyses.

Temperature dependent X-ray diffraction (XRD) experiments were conducted at the materials science synchrotron beamline for energy-dispersive diffraction [7] at BESSY in Berlin, Germany. White synchrotron radiation with an energy range from ~ 20 to 100 keV and symmetric $\Theta/2\Theta$ configuration with $2\Theta = 12^\circ$ and $\omega = 6^\circ$ were used. The film material powders were filled into borosilicate glass capillaries and clamped on a heating plate of a Domed Hot Stage DHS1100 (Anton Paar GmbH). A thermocouple embedded in the powder material inside the glass capillaries was used to monitor the actual powder temperature. The powders were directly heated in nitrogen gas atmosphere (to avoid oxidation) up to 600°C (without XRD data collection) to allow for growth defect annihilation and stepwise cooled back down to room temperature using temperature steps of $\Delta T = 50^\circ\text{C}$. At each temperature step in the cooling down process, an energy-dispersive diffraction pattern was collected (acquisition time per pattern = 60 s). Another stepwise heating up and cooling down cycle was performed to proof reproducibility and to ensure that no phase transformations (e.g., decomposition of the supersaturated phases) occurred within the thermocycles. The maximum temperature of 600°C was chosen to be clearly below the onset of thermally activated decomposition starting above $\sim 800^\circ\text{C}$ for Ti-Al-N [3] and $\sim 925^\circ\text{C}$ for Cr-Al-N [8].

The diffraction patterns were analyzed using an energy dispersive Rietveld analysis program provided by the beamline staff [9,10]. All films studied exhibited the B1 structure with (room temperature) lattice parameters being in excellent agreement with predictions from Refs. [11,12]. The experimentally determined lattice parameters for TiN, $\text{Ti}_{0.45}\text{Al}_{0.55}\text{N}$, CrN, $\text{Cr}_{0.52}\text{Al}_{0.48}\text{N}$, $\text{Cr}_{0.40}\text{Al}_{0.60}\text{N}$, and $\text{Cr}_{0.31}\text{Al}_{0.69}\text{N}$ are 4.2339, 4.1773, 4.1502, 4.1255, 4.1171, and 4.1113 Å, respectively. The temperature dependent TECs were derived from the temperature dependent lattice parameters by fitting the data with a polynomial function and using the definition of the thermal expansion coefficient: $\text{TEC}(T) = \frac{1}{\alpha(T)} \frac{d\alpha}{dT}$.

The quantum mechanical calculations of TECs were performed using Density Functional Theory [13,14] as implemented in the Vienna Ab initio Simulation Package (VASP) [15]. The plane wave cut-off energy was set to 500 eV. The exchange and correlation effects were described within both LDA (known to overestimate binding) and PW91-GGA [16] (typically underestimating binding), hence providing upper and lower estimates for thermodynamic properties [17]. Our test calculations additionally showed only insignificant differences between PW91-GGA and PBE-GGA [18] calculations, hence making the present data comparable with other literature [19]. The electron-ion interactions were described using the PAW pseudopotentials [20] (Al, Ti_{pv}, N). The simulation supercells were composed of $2 \times 2 \times 2$ conventional rock-salt cubic cells (64 atoms) and $2 \times 2 \times 2$ wurtzite unit cells (32 atoms) [16,17,18,20]. The chemical disorder of our supercells was treated using Special Quasi-random Structures [21], with the pair short-range order parameters optimized up to 7th nearest neighbour shell (the exact supercell configuration of our wurtzite cells was described earlier in Ref. [22]). The Brillouin zones of the cubic and wurtzite structures were sampled with $5 \times 5 \times 5$ and $8 \times 8 \times 4$ k-points, respectively.

The phonopy code [23] was used to evaluate the Helmholtz free energies, and further to calculate the Gibbs free energy within the framework of the quasi-harmonic approximation (QHA) applied to 8 volumes evenly distributed from 96% to 110% of the 0 K equilibrium volume. The Gibbs free energy subsequently allowed determination of the TECs of respective coating materials. The TEC of CrN [19] and B1 AlN [24] are taken from our recently published ab initio calculations.

Figs. 1 and 2 present the experimentally derived (data points) and theoretically predicted (solid and dashed lines) TECs of $\text{Ti}_{1-x}\text{Al}_x\text{N}$ and $\text{Cr}_{1-x}\text{Al}_x\text{N}$ alloys, respectively. While the experimentally found TECs for TiN and $\text{Ti}_{0.45}\text{Al}_{0.55}\text{N}$ are only slightly increasing with increasing Al content, a more pronounced compositional spread is observed for the $\text{Cr}_{1-x}\text{Al}_x\text{N}$ alloys. For the latter, the TECs and their temperature dependence significantly increase with increasing Al content. The measured values are in good qualitative agreement with the ab initio predictions, and in the case of the LDA (solid lines in the Figs. 1 and 2) they agree excellently also quantitatively. Oxygen and other impurities influencing the microstructure and bonding characteristics could be one reason for the slight differences between theory and experiment. The GGA (dashed lines in the Figures) leads to slightly overestimated TEC values, a trend consistent with the analysis of pure CrN in Ref. [19]. The compositional spread is more pronounced in the case of the LDA showing an increase of the TEC with increasing Al contents. The TECs found in this study are in good agreement with literature values reported for TiN and CrN in Refs. [4,25,26]. Tkadletz et al. [27] reported the same compositional trend for TiAlN, i.e. slightly larger TEC values for TiAlN as compared with TiN, however, the authors there found lower absolute TEC values.

The ab initio TEC of wurtzite type B4 AlN is also added to Figs. 1 and 2 for comparison. The differences between GGA (dotted and dotdashed lines) and LDA (solid line) calculations are only small and there are no significant differences between calculations with fixed c/a ratio (dotdashed line) and optimized (volume dependent) c/a ratio (dotted line) using $\alpha_a = \frac{1}{3}\alpha_v$. Importantly, the TEC of B4 AlN is significantly smaller than that of cubic B1 AlN (with $\text{TEC}_{\text{B4-AlN}} \sim 0.5 \cdot \text{TEC}_{\text{B1-AlN}}$ for temperatures between ~ 200 and 680°C). Based on these results, we

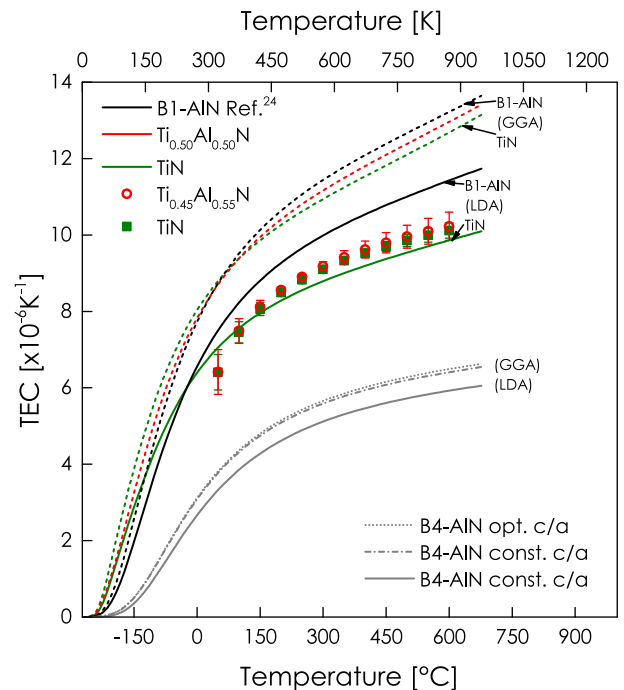


Fig. 1. Temperature dependent TEC of B1 Ti-Al-N alloys and B4 AlN. The solid lines correspond to the LDA, the dashed, dotted and dotdashed lines to the GGA, whereas the data points were derived from the synchrotron experiments.

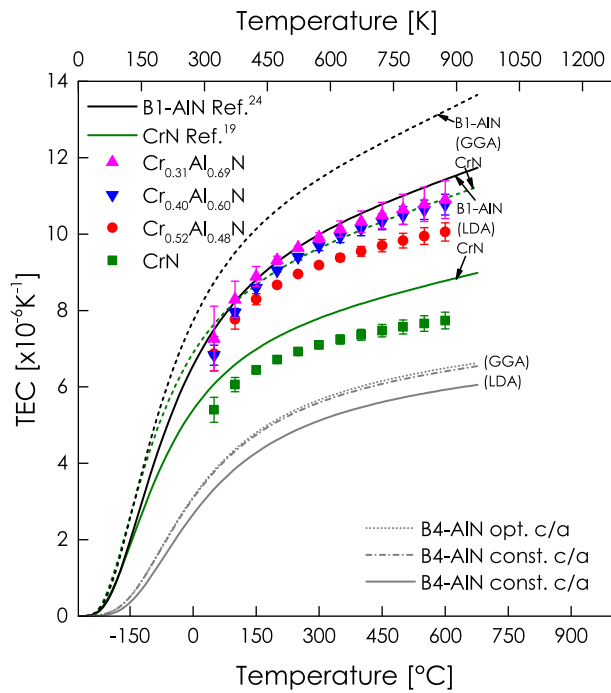


Fig. 2. Temperature dependent TEC of B1 Cr-Al-N alloys and B4 AlN. The solid lines correspond to the LDA, the dashed, dotted and dot-dashed lines to the GGA, whereas the data points were derived from the synchrotron experiments.

suggest that also the B4 counterpart of the cubic B1 ternaries $Ti_{1-x}Al_xN$ and $Cr_{1-x}Al_xN$ exhibit significantly smaller TECs. As a consequence of this mismatch, pronounced thermal stresses are formed upon temperature changes in $Ti_{1-x}Al_xN$ and $Cr_{1-x}Al_xN$ films as soon as they comprise B1 and B4 phases. Such compounds can be formed due to the preparation of these ternaries with chemical compositions close to their metastable solubility limit, hence, with Al contents x close to 0.7, or due to thermally activated decomposition of their supersaturated cubic phases towards B1 TiN and B4 AlN, respectively B1 CrN and B4 AlN. The significant difference between the thermal expansion of the cubic (B1) and the wurtzite (B4) phase may also influence the thermal stability of $Ti_{1-x}Al_xN$ and $Cr_{1-x}Al_xN$ based coatings, as the phase with the larger volume (B4) expands less with increasing temperature than the phase with the smaller volume (B1). Consequently, for $Ti_{1-x}Al_xN$ and $Cr_{1-x}Al_xN$ thin films containing already B4 structured phases within their as-deposited state, the formation of B4 AlN is additionally (to the already existing B4 nuclei) promoted. The lower TEC of the B4 structured phases (embedded in B1 structured matrix) will generate tensile stresses, which themselves promote the decomposition of the supersaturated B1 structured matrix towards B1 TiN (respectively CrN) and the more spacious B4 AlN.

The reasons for the large difference in the expansion coefficients of cubic and hexagonal AlN may originate for example from the larger specific volume of the wurtzite phase compared to that of the cubic phase (~26% larger) as the TEC is inversely proportional to volume. Another reason might be that the bonds in B4-AlN have presumably more covalent character (sp^3 bonding) than in cubic AlN (B1 transition metal nitrides exhibit sp^3d^2 hybridization; however, since AlN is missing any d electrons, only weaker s-p hybridization appears). Consequently, B4 exhibits stronger bonds than B1 (also reflected by the more negative energy of formation of B4 than of B1). Hence, one may expect smaller expansion of B4 than that of B1.

For physical vapor deposited thin films, not just their chemical composition and crystal structure are crucial but also their defect structure, as they typically exhibit a high content of point and line defects stemming from the film growth process. Their influence on the TEC is exemplarily studied for TiN by performing synchrotron measurements during

three thermocycles, where the maximum temperature T_{max} of each subsequent thermocycle is higher than that of the preceding. The (as-deposited) TiN powder was measured during a first thermocycle up to $T_{max,1} = 300$ °C, being also the deposition temperature T_{dep} . During this first cycle, the lattice parameter difference Δa (relative to the lattice parameter of the as-deposited film material) changes almost linearly with temperature T and no significant change between heating and cooling segment can be detected, Fig. 3a, indicating no significant recovery of built-in structural defects (like point and line defects). Hence, also the microstrain ε (intrinsic strains between individual grains or columns (second order) and within these microstructural features such as point and line defects (third order)) is constant with temperature during this first thermocycle, Fig. 3b. This is because the maximum temperature was the deposition temperature; hence, any defect generated during film growth – and not annealed-out immediately during the deposition process – requires a higher temperature to migrate. Here we also want to mention, that film growth processes are dominated by surface diffusion processes, which are anyhow faster and easier than grain boundary and especially bulk diffusion processes [28]. For a grown thin film, the major diffusion mechanisms are grain boundary and bulk diffusion. Therefore, temperatures above the deposition temperature are needed during a post-deposition annealing treatment, to allow for diffusion related phenomena. This in turn explains that during the heating segment of the second thermocycle (with a maximum temperature $T_{max,2}$ of ~450 °C), performed immediately after the first, no significant change in the a -vs- T and ε -vs- T behaviour can be detected up to the maximum temperature $T_{max,1}$ of the previous cycle, Fig. 3a.

Annealing at temperatures above T_{dep} provides sufficient diffusion to allow for recovery processes of built-in structural defects, resulting in a significant deviation from the thermoelastic behaviour of the a -vs- T curve, Fig. 3a. During these recovery processes, the TEC is significantly reduced. This flattening of the a -vs- T curve indicates thermally activated recovery of these kinds of defects and defect combinations that lead to a smaller lattice parameter when they are healed out. DFT simulations proof that only vacancies lead to decreasing lattice parameters, other point defects like interstitials, Schottky defects or even anti-site occupation cause the lattice parameter to increase [29]. During cooling down, the a -vs- T curve again approaches the (almost linear) thermoelastic behaviour suggesting that no further recovery processes are active, especially for $T \leq 400$ °C. Rietveld analysis of the collected powder diffraction patterns revealed that the decrease in peak broadening – upon annealing above the deposition temperature – originates exclusively from microstrain reductions (i.e., recovery processes of the structure towards lower energy configuration of their built-in point and line defects), Fig. 3b, while the coherently diffracting domain size remains constant (i.e., no grain growth occurred). The third thermocycle shows a comparable behaviour with recovery onset when exceeding $T_{max,2}$.

The temperature dependent lattice parameter data sets from the cooling sequences of the individual thermocycles were used to determine the thermal expansion coefficients of our TiN thin films as a function of T , Fig. 3c. As the maximum annealing temperature increases from thermocycle 1 to 2 to 3, and thus the microstrain decreases (Fig. 3b), the defect content decreases and adopts lower energy sites. Especially the TEC of our 550 °C annealed TiN thin film – obtained from the cooling segment of the thermocycle 3 ($T_{max,3} = 550$ °C) – excellently agrees with LDA calculations of defect-free TiN. Contrary, the TEC of our 450 °C and 300 °C annealing TiN thin film significantly deviates showing larger TEC values. Hence, the agreement between experiment and calculations – also with regard to the temperature dependence of the TEC (Fig. 3c) – is the better the lower defect content in film material.

The larger TEC of defected TiN is reflected in the interatomic potentials, which become more asymmetric for defected TiN as compared to defect-free TiN. Fig. 3d compares the interatomic potentials for defect-free TiN, $Ti_{32}N_{31}$ [1 N vacancy] and $Ti_{31}N_{32}$ [1 Ti vacancy] at 0 K showing that the effect is more pronounced for N than for Ti vacancies.

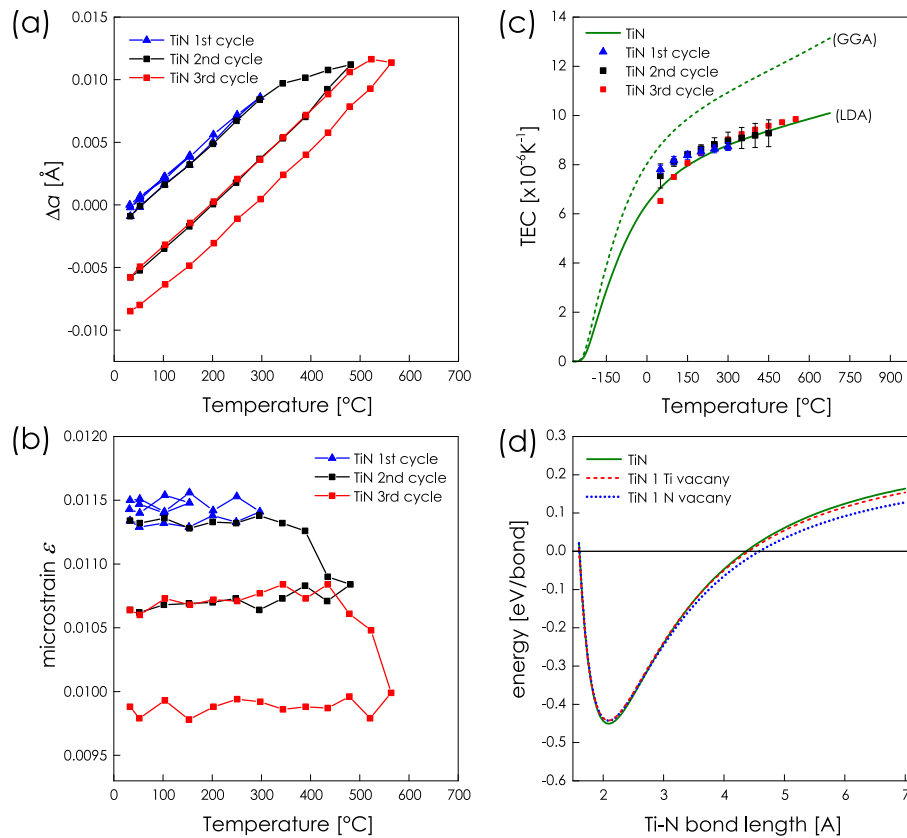


Fig. 3. Temperature dependent lattice parameter (a) and microstrain (b) evolution during thermocycling of B1 TiN. The influence of point defects on TEC is shown in (c). The solid lines correspond to the LDA, the dashed line to the GGA, the data points were derived from the synchrotron experiments. In (d) the interatomic potentials of defect-free and defected TiN crystal lattices are compared using the LDA.

Based on our results, and especially the excellent agreement between experiments and ab initio calculations, we can conclude, that the temperature dependent thermal expansion coefficients of cubic B1 structured $Ti_{1-x}Al_xN$ and $Cr_{1-x}Al_xN$ coatings increase with increasing Al content. This increase is marginal for $Ti_{1-x}Al_xN$ but significant for $Cr_{1-x}Al_xN$. Coatings with as-deposited built-in structural defects exhibit higher TECs with a lower temperature dependence than their 600 °C annealed counterparts and ab initio calculations. The combination of first principle simulations and experimental synchrotron diffraction experiments provides a reliable data basis, which can be used for thermal stress calculations. Residual stresses in turn are a key aspect for prolonging the lifetime of Ti-Al-N and Cr-Al-N based coated engineering components.

The financial support by the Austrian Federal Ministry of Economy, Family and Youth and the National Foundation for Research, Technology and Development is gratefully acknowledged. We also thank for the financial support of Plansee Composite Materials GmbH and Oerlikon Balzers, Oerlikon Surface Solutions AG. The financial support by the START Program (Y371) of the Austrian Science Fund (FWF) is highly acknowledged. The computational results presented have been achieved using the Vienna Scientific Cluster (VSC). The authors thank the Helmholtz Zentrum Berlin for the allocation of synchrotron radiation beamtime.

References

- [1] S. PalDey, S.C. Deevi, *Mater. Sci. Eng.* A342 (2003) 58.
- [2] A.E. Reiter, V.H. Derflinger, B. Hanselmann, T. Bachmann, B. Sartory, *Surf. Coat. Technol.* 200 (2005) 2114.
- [3] P.H. Mayrhofer, A. Hörling, L. Karlsson, J. Sjölin, T. Larsson, C. Mitterer, L. Hultman, *Appl. Phys. Lett.* 83 (2003) 2049.
- [4] L.B. Freund, S. Suresh, *Thin Film Materials: Stress, Defect Formation, and Surface Evolution*, Cambridge University Press, Cambridge, United Kingdom, 2003.
- [5] A. Bastia, T. Obikawa, J. Shinozuka, *Int. J. Mach. Tools Manuf.* 47 (2007) 793.
- [6] M. Bartosik, R. Daniel, Z. Zhang, M. Deluca, W. Ecker, M. Stefanelli, M. Klaus, C. Genzel, C. Mitterer, J. Keckes, *Surf. Coat. Technol.* 206 (2012) 4502.
- [7] C. Genzel, I.A. Denks, J. Gibmeier, M. Klaus, G. Wagener, *Nucl. Inst. Methods A* 578 (2007) 23.
- [8] H. Willmann, P.H. Mayrhofer, P.O.Å. Persson, A.E. Reiter, L. Hultman, C. Mitterer, *Scr. Mater.* 54 (2006) 1847.
- [9] D. Apel, M. Klaus, C. Genzel, D. Balzar, *Z. Kristallogr.* 226 (2011) 934.
- [10] D. Apel, M. Klaus, M. Genzel, C. Genzel, *J. Appl. Crystallogr.* 47 (2014) 511.
- [11] L. Zhou, D. Holec, P.H. Mayrhofer, *J. Appl. Phys.* 113 (2013) 043511.
- [12] D. Holec, R. Rachbauer, L. Chen, L. Wang, D. Luef, P.H. Mayrhofer, *Surf. Coat. Technol.* 206 (2011) 1698.
- [13] P. Hohenberg, W. Kohn, *Phys. Rev.* 136 (1964) B864.
- [14] W. Kohn, L.J. Sham, *Phys. Rev.* 140 (1965) A1133.
- [15] G. Kresse, J. Furthmüller, *Comput. Mater. Sci.* 6 (1996) 15.
- [16] Y. Wang, J.P. Perdew, *Phys. Rev. B: Condens. Matter Mater. Phys.* 44 (1991) 13298.
- [17] B. Grabowski, T. Hickel, J. Neugebauer, *Phys. Rev. B* 76 (2007) 024309.
- [18] J.P. Perdew, K. Burke, M. Ernzerhof, *Phys. Rev. Lett.* 77 (1996) 3865.
- [19] L. Zhou, F. Körmann, D. Holec, M. Bartosik, B. Grabowski, J. Neugebauer, P.H. Mayrhofer, *Phys. Rev. B* 90 (2014) 184102.
- [20] G. Kresse, D. Joubert, *Phys. Rev. B: Condens. Matter Mater. Phys.* 59 (1999) 1758.
- [21] S.-H. Wei, L.G. Ferreira, J. Bernard, A. Zunger, *Phys. Rev. B Condens. Matter* 42 (1990) 9622.
- [22] L. Chen, D. Holec, Y. Du, P.H. Mayrhofer, *Thin Solid Films* 519 (2011) 5503.
- [23] A. Togo, F. Oba, I. Tanaka, *Phys. Rev. B* 78 (2008) 134106.
- [24] M. Bartosik, M. Todt, D. Holec, J. Todt, L. Zhou, H. Riedl, H.J. Böhm, F.G. Rammerstorfer, P.H. Mayrhofer, *Appl. Phys. Lett.* 107 (2015) 071602.
- [25] K. Aigner, W. Lengauer, D. Rafaja, P. Ettmayer, *J. Alloys Compd.* 215 (1994) 121.
- [26] R. Daniel, D. Holec, M. Bartosik, J. Keckes, C. Mitterer, *Acta Mater.* 59 (2011) 6631.
- [27] M. Tkadletz, N. Schalk, R. Daniel, J. Keckes, C. Czettel, C. Mitterer, *Surf. Coat. Technol.* 285 (2016) 31.
- [28] L.-C. Dufour, C. Monty, G. Petot-Ervas, *Surfaces and Interfaces of Ceramic Materials*, Kluwer Academic Publishers, 1989.
- [29] N. Koutná, Master Thesis, Masaryk University, Brno, 2016.